Materials and Design 121 (2017) 262–271

Contents lists available at ScienceDirect

Materials and Design

journal homepage: www.elsevier.com/locate/matdes

Novel processing of Ag-WC electrical contact materials using spark plasma sintering

Nachiketa Ray [a,*], Bernd Kempf [b], Gunther Wiehl [b], Timo Mützel [b], Frank Heringhaus [b], Ludo Froyen [a], Kim Vanmeensel [a], Jef Vleugels [a]

[a] KU Leuven, Department of Materials Engineering, Kasteelpark Arenberg, 44, 3001 Heverlee, Belgium
[b] Umicore AG & Co. KG, Rodenbacher Chaussee 4, 63457 Hanau-Wolfgang, Germany

HIGHLIGHTS

- Novel processing of Ag-WC (60-40 wt%) contact materials by spark plasma sintering (SPS)
- Single-step material densification and in-situ joining to copper substrate
- Faster processing at lower temperatures
- SPS composites are more homogeneous, tougher and softer than conventionally processed equivalents.

GRAPHICAL ABSTRACT

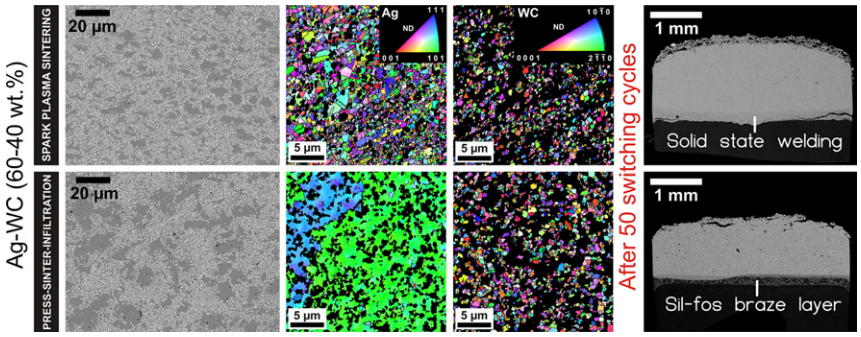

ARTICLE INFO

Article history:
Received 16 November 2016
Received in revised form 20 February 2017
Accepted 21 February 2017
Available online 24 February 2017

Keywords:
Metal matrix composites
Powder metallurgy
Spark plasma sintering
In-situ joining
Flexural strength
Electron backscattered diffraction

ABSTRACT

Ag-WC (60-40 wt%) contact materials based on three WC particle size powders were doped with 0.1 wt% Ni and processed by an appropriate powder pre-treatment followed by spark plasma sintering (SPS). The contacts produced were already bonded to a copper profile during SPS in order to eliminate additional processing steps. The SPS composites had a more homogeneous microstructure and were tougher and softer than the materials produced by conventional press-sinter-infiltration. The infiltrated contacts had a lower arc-erosion whereas the contacts produced by both processes had a similar contact resistance. The microstructure after switching confirmed that the SPS materials had a porous contact surface layer and were crack-free in contrast to their press-sinter-infiltrated equivalents.

1. Introduction

Silver based refractory metal/metal carbide composites are used as an arc resistant contact material for low-voltage molded case circuit breakers (MCCBs) and miniature circuit breakers (MCBs) [1,2]. These contact materials must be able to withstand extreme arcing conditions generated by a short circuit with minimal material loss, should have

* Corresponding author.
E-mail addresses: nachiketa.ray@kuleuven.be, nachiketa.ray.1014@gmail.com (N. Ray).

http://dx.doi.org/10.1016/j.matdes.2017.02.070
0264-1275/

acceptable contact resistance at 'rated' currents after arcing and should not weld to each other at high currents. This set of stringent conditions is only fulfilled by carefully engineered metal-ceramic composites, which can comply with independent material properties like superior conductivity and high boiling point. Conventionally, Ag-WC composites are produced by liquid phase sintering or press-sinter-infiltration [3–5] which requires a good adherence between the metallic and ceramic phase which otherwise have limited solubility in both solid and liquid state [6].

A novel approach has being adopted recently to prepare these metal matrix composites in a single step process using pressure assisted pulsed electric current sintering, commonly known as spark plasma sintering (SPS). This approach has recently been used to prepare Ag-SnO_2 electrical contacts [7,8], W-Cu-Ni contacts [9] and Ag-WC (40-60) contacts for vacuum contactors [10]. This process allows drastically reducing the sintering time, since a very fast heating and cooling rate can be achieved. In spark plasma sintering, the densification is mostly carried out in the solid state, thus limiting the sintering temperature to the liquidus of the powder mixture, which otherwise would lead to exudation of the liquid phase during the process [11]. Since sintering is predominantly carried out in the solid state, the homogenization of multiple phases present is limited to solid state diffusion. Therefore, the powder mixing step is critical as it directly reflects the homogeneity and microstructure of the final composite.

Tsakiris et al. [10] have only achieved 95% of the theoretical density for Ag-WC 40-60 materials after sintering at high homologous temperatures ($T/T_{m\ silver} \approx 0.98$). Such high homologous temperatures during SPS involves the risk of exudation of silver, and deprives the possibility of achieving higher composite silver contents. Therefore, in order to have a stable production and to achieve higher silver contents, sintering at lower temperatures is required. In the electrical industry, the attachment of an electrical contact to the contact arm has been of considerable interest especially because of the difficulty of joining the refractory phase in the composite to a copper or steel substrate. Joining of the contacts to a copper profile is commonly achieved by positioning a silver solder (sil-fos) in-between the composite and copper [12–14], followed by resistance brazing. This process however demands an extra step which can be eliminated by solid state welding of the composite to the copper plate.

Therefore, the feasibility to fabricate Ag-WC-Ni (60-39.9-0.1 wt%) electrical contact materials directly on a copper support in the solid state at 750 °C has been investigated in this work. From previous investigations it was established that both the Ag content and WC particle size have a strong influence on the electrical contact resistance and thermal conductivity of Ag-WC composites [15]. Therefore, in this work the WC particle size was varied between 0.8 μm, 1.5 μm and 4 μm. A composition of Ag-WC (60-40 wt%) was chosen since these composites are used as arcing contacts in low-voltage molded case circuit breakers (MCCBs) and power circuit breakers, which uses a similar composition [2]. The material stability in the liquid state at 1070 °C was assessed and the mechanical properties (hardness, toughness, yield strength and flexural failure strength) and switching properties (arc-erosion and contact resistance) of the SPS and infiltrated materials based on three different WC starting powder particle sizes are compared.

2. Experimental approach

2.1. Powder mixing and treatment

Ag-WC-Ni (60-39.9-0.1 wt%) composites were prepared via powder metallurgical routes by powder mixing, followed by densification. The silver and nickel powders used had a median particle diameter (d_{50}) of 5 μm and 7 μm respectively. Different powder batches were prepared by varying the WC particle size between 0.8 μm, 1.5 μm and 4 μm. All powders were obtained from Umicore AG & Co. KG, Germany. 100 g of powder was suspended in 100 ml demineralized water in a glass beaker using a magnetic stirrer for ~5 min. The stirred suspension was subsequently poured into a horizontal bead mill (Dispermat SL-12C1, VMA Getzmann GmbH, Germany) containing WC-6Co Ø 1 mm milling beads (YG6, Zhuzhou Jingzuan Carbide Co., Ltd.) and mixed for 15 min at 1000 rpm. The purpose of this step was to de-agglomerate and mix the powders homogeneously. The time and mixing speed was categorically achieved by optimizing the final microstructure from a series of mixing experiments. Silver is very ductile and has the propensity of forming flakes, which is undesirable for the final microstructure. A longer mixing time and/or a higher mixing speed would result in a microstructure consisting of elongated silver phases with embedded WC particles. The mixed suspension was dried using a rotary evaporator, and the thus obtained soft agglomerated powder was sieved through a 300 μm sieve. It is important to note that the composition of the composite can be easily controlled by the powder composition in this process, which is a major drawback of the conventional press-sinter-infiltration process, where the final silver content needs to be tediously manipulated from the sinter shrinkage as explained in Section 2.3. In order to remove all oxides in the as-mixed powder, a hydrogen reduction step was performed in a tube furnace at 945 °C for 8 h under a pure dry hydrogen flow of 50 l/h. Since the Ag-WC powder mixture

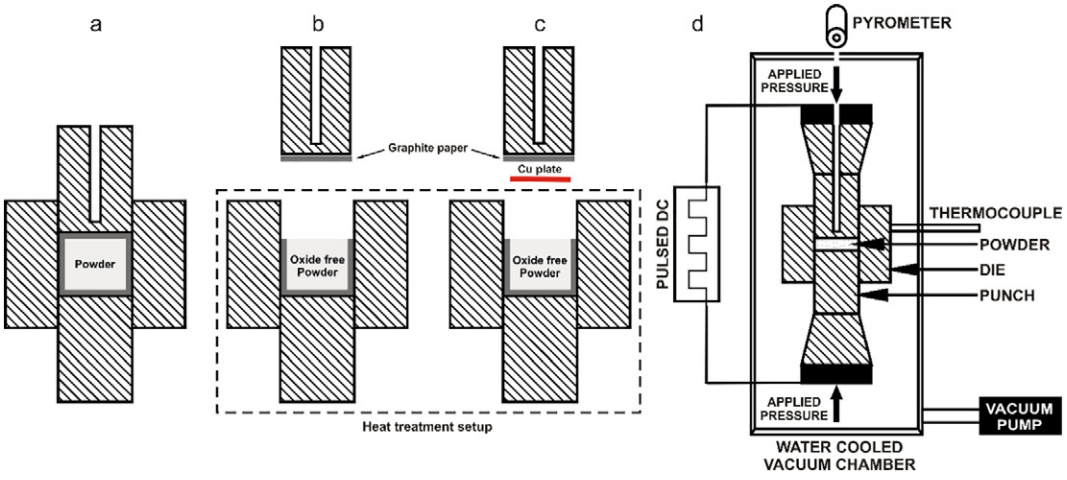

Fig. 1. Die-punch-powder configurations (a, b, c) and schematic of the spark plasma sintering set-up (d). Configuration (a) was as-mixed powder without any heat treatment, whereas configuration (b) and (c) were heat treated under hydrogen atmosphere. Configuration (a) and (b) were sintered according to the profile shown in Fig. 2(a) (i.e. 850 °C and 80 MPa) and configuration (c) was sintered according to the profile shown in Fig. 2(b) (i.e. 750 °C and 80 MPa).

would sinter together at such high temperatures, the powders were heat treated directly in the graphite SPS dies, as shown in Fig. 1(b) and (c). The upper punch was removed during the hydrogen reduction in order to allow direct access of the gas to the powder.

2.2. Densification by spark plasma sintering

25 g of the as-mixed and sieved powder mixture was poured into a graphite die punch set-up (Ø 30 mm) with graphite paper positioned (Sigraflex N 998) around the powder mixture (Fig. 1(a)). The set-up was uniaxially cold pressed at 7 MPa so that the punches made thorough contact with the powder. Alternatively, the powder compact was hydrogen treated inside the graphite die/punch set-up prior to SPS densification, as specified above and schematically presented in Fig. 1(b). The punch/powder/die set-up was placed inside the SPS vessel between the electrodes and sintered at 850 °C under a pressure of 80 MPa according to the profile (a, blue) shown in Fig. 2. Both the as-mixed powder and hydrogen reduced powder mixture were densified under identical sintering conditions and both showed no significant difference in sintering shrinkage. The vacuum was maintained at 1 mbar during the process. A series of experiments was performed to obtain the sintering parameters without any risk of exudation. A temperature of 850 °C was sufficient to achieve near theoretical density under a pressure of 80 MPa. The applied pressure was also limited by the strength of the graphite punches. A schematic of the SPS (Type HP D 25/1, FCT Systeme, Frankenblick, Germany) is shown in Fig. 1(d). More details of the experimental set-up are provided elsewhere [16].

In a second approach, the hydrogen reduced powder was directly SPSed on a copper substrate. After hydrogen reduction, a flat copper plate (Ø 30 mm, 2 mm thick) was placed on the powder bed, on which the upper punch was placed, as illustrated in Fig. 1(c). The sintering of this configuration was carried out at 750 °C under a pressure of 80 MPa as shown in the profile (b, red) in Fig. 2. After the 30 mm disc was densified, the remnants of the graphite paper sticking to the composite were removed by sand blasting.

2.3. Reference materials: densification by conventional infiltration

In order to evaluate the contacts prepared by SPS, they were compared with 0.1 wt% Ni doped Ag-WC (60-39.9 wt%) contacts prepared by the conventional press-sinter-infiltration method. In this process, a starting powder composition of 40 wt% Ag, 59.85 wt% WC and 0.15 wt% Ni was mixed in a bead mill in the same way as for the SPS materials. The resultant powder mixture was used to make green pellets of Ø 7 mm by uniaxial pressing. These pellets were sintered at 970 °C for 30 min to yield a porous body. The density of this sintered body was measured in order to estimate the amount of porosity. In this case, the desired silver content was 60 wt% in the final composition, thus the pressure during uniaxial pressing was optimized in order to ensure enough porosity after sintering to accommodate the remaining silver. The sintered pellets were infiltrated with silver at 1070 °C for 30 min which allowed the composite to achieve a near theoretical density (>99%). Both sintering and infiltration were carried out above the melting point of silver in a graphite crucible and a reducing H_2:N_2 (3:1) atmosphere in order to prevent oxidation of the tungsten carbide.

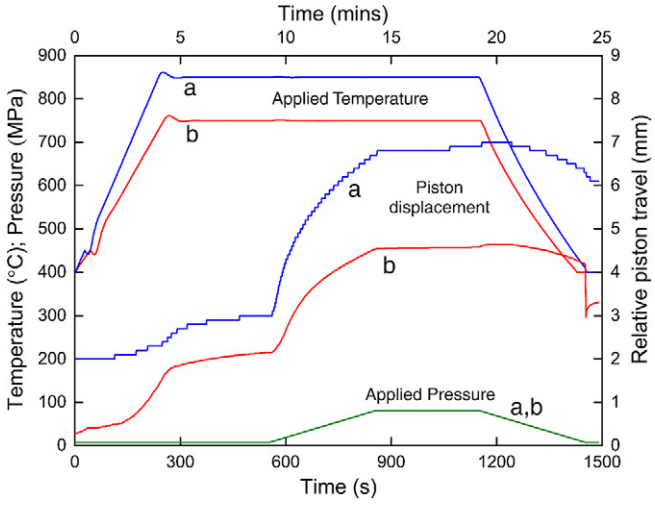

Fig. 2. Applied temperature and pressure profile and concomitant piston movement, representing the linear shrinkage of the Ag-WC(0.8 μm)-Ni compact during spark plasma sintering. (a) As-mixed or hydrogen reduced powder compact and (b) hydrogen reduced powder compact on a copper plate substrate.

2.4. Characterization

The density of the sintered composites was measured according to the Archimedes' principle in water, whereas the density of the porous materials was measured applying the boiling water method explained in [17]. Three-point bending testing was used to determine the flexural strength of the Ag-WC composites on a universal testing machine (5848 Micro Tester; Instron, Norwood, MA, USA) using a set-up with a span length of 10 mm. A 500 N load cell and a crosshead velocity of 0.05 mm/min was used in all tests. The details of the test set-up can be found in [18]. The densified composites produced by SPS and infiltration were machined and ground into bars of 12 × 2 × 1.5 mm dimension. Seven samples were tested for each material grade. The yield strength was calculated as the proof stress at 0.2% offset strain. The toughness, i.e. the energy of deformation per unit volume prior to fracture, was determined by integrating the flexural stress-strain curves. The Vickers hardness of the Ag-WC composites was measured (Model FV-700, Future-Tech Corp., Tokyo, Japan) using a load of 0.3 kg and a dwell time of 10 s. The reported values are the average and standard error of mean of five indentations.

The transverse section of the contact was used for microstructural characterization, i.e., the plane perpendicular to the contact surface. Scanning electron microscopy (XL 30 FEG, FEI) was used for investigating the initial and post-switching microstructures. Wavelength-dispersive X-ray spectroscopy (WDS) elemental mapping of the Ag-WC-Ni contact and the copper interface was performed using Electron probe micro-analysis (EPMA, JXA-8530F, JEOL). Electron backscattered diffraction (EBSD) (Nova NanoSEM 450, FEI) was used to measure orientation data in order to calculate grain size and grain boundary character. The step size for the EBSD scans was varied from 0.05–0.1 μm, which was determined by the grain size. The orientation data obtained from the EBSD scan was analyzed using EDAX OIM™ Analysis Software.

2.5. Break-only model switch test

The fully densified discs (Ø = 30 mm, h = 3 mm) were machined into smaller (Ø = 7 mm) discs using electrical discharge machining (EDM). The composites densified on a copper substrate were brazed using 'sil-fos 15' (Ag-Cu-P 15-80-5 wt%) on a copper rod (40 mm × Ø 8 mm) at 750 °C and further machined to 4 mm diameter for the break-only switching test, explained in detail in [15,19]. In this test, a half sinusoidal current wave, having a frequency of 50 Hz and peak current of 1300 A was applied across an identical material pair in contact. At the beginning of the sine wave (i.e. $i = 0$), the contacts were pulled apart causing an arc discharge between the two contact materials until the next current zero. After the arc was extinguished, the contacts were brought together and a direct current of 10 A was applied across them. The voltage drop measured was used to calculate the electrical contact resistance (R_c) of the composite after arcing. This controlled sequence was repeated 50 times (cycles) providing an evolution of the R_c with increasing arc damage on the contact surface. The total time for 50 cycles was 4 min, i.e., 4.8 s per cycle. Apart from the contact

Table 1
Density of SPS and thermally treated SPS Ag-WC composites as a function of the starting powder mixture treatment prior to SPS.

Powder treatment in H_2		Relative density after SPS (%)	Heat treatment for 1 h		Relative density after heat treatment (%)
Temperature (°C)	Time (min)		Temperature (°C)	Atmosphere	
–	–	98.35	990	H_2:N_2 3:1	62.91
–	–	98.35	1070	H_2:N_2 3:1	62.62
–	–	98.35	1070	Pure N_2	71.57
945	26	98.97	1070	H_2:N_2 3:1	81.18
945	480	99.07 ± 0.35	1070	H_2:N_2 3:1	99.23 ± 0.62

resistance, the arc-erosion of the contacts after 50 cycles was measured as the total weight loss after switching. The contact resistance measurement system was fully automated, and had minimal operator influence. The arc-erosion measurement was carried out in a high precision mass balance up to 6 significant digits. Two contact pairs (4 samples) for each case were tested and reported in this work. In order to test the repeatability of the switching device over time, a standard known sample was tested before each set of experiments. The absolute values of resistance and erosion are valid for the given test conditions and would change for different test conditions.

3. Results and discussion

3.1. Densification and thermal stability

Since sintering of the composites was carried out below the melting point of silver, the wettability of silver on tungsten carbide was not deterrent for densification. Table 1 summarizes the density of three Ag-WC-Ni (60-39.9-0.1 wt%) composite materials prepared via SPS with a WC particle size of 0.8 μm with or without hydrogen powder treatment. The density after solid state sintering for all composites are close to their theoretical density. However, the application temperatures of the contact material in a circuit breaker are well beyond the melting point of silver [20]. Thus it is crucial to assess the thermal stability of the solid state densified SPS materials above the melting point of silver.

Sectioned parts of the SPS densified composites were placed in a graphite crucible in a tube furnace at 990 °C or 1070 °C under different atmospheres and the change in density of the SPS composites is summarized in Table 1. During heat treatment under reducing or N_2 atmosphere, all as-mixed powder based SPS composites inflated, as confirmed from the decreased relative theoretical density (Table 1) and microstructure shown in Fig. 3. The large amount of porosity was corroborated to the formation of water vapor and/or volatile oxides and oxide hydrates [$WO_2(OH)_2$] of tungsten [21,22] during heat treatment. The tungsten carbide phase present in the as-milled powder based dense SPS composites was partially oxidized. Heat treatment in a hydrogen containing atmosphere leads to the reduction of the tungsten oxides into tungsten and water vapor, which is either transferred to the environment or internally builds up a partial pressure. Increasing the temperature leads to an expansion of the gases which results in the formation of 'macro' pores which are visible to the bare eye. In the absence of hydrogen, no water vapor formation is anticipated, but tungsten oxides evaporate at elevated temperatures (800–1200 °C) [21,22] which in turn generates porosity. The porosity after heat treatment in a reducing atmosphere is substantially higher than in N_2, as summarized in Table 1, due to the release of both water vapor and volatile tungsten oxides.

It is evident from Table 1 that a pre-treatment of the powder in hydrogen at 945 °C prior to SPS densification reduces all the oxides present before sintering, eliminating the oxide content in the SPS composite and concomitantly avoids pore formation during subsequent heat treatment at 1070 °C. In the present work, 8 h of powder pre-treatment in hydrogen allowed to eliminate all possible oxides present in the powder mixture. This method allowed to make dense composites of desired composition by a combined hydrogen reduction powder treatment and spark plasma densification, which also eliminates the multiple stages and complications characteristic for the press-sinter-infiltration methods [4].

3.2. In-situ joining of Cu and Ag-WC-Ni composite during SPS

In this work, the hydrogen reduced starting powder mixture was directly 'SPS joined' to a pure copper substrate at 750 °C, a temperature below the Ag-Cu eutectic temperature (779 °C) in order to avoid exudation during sintering, the individual melting points of Ag and Cu being 962 °C and 1085 °C respectively. The thermal and loading cycle are provided in Fig. 2(b). In 2015, Fu et al. developed a different technique of vacuum plasma deposition of Ag-WC (40-60 wt%) powders on a copper substrate to achieve a similar Ag-WC contact material with a copper base [23].

Although heating the powder and the copper plate below the Ag-Cu eutectic temperature does not allow liquid phase formation, the copper and silver become very soft and plastically deformed. In addition to electric resistance welding, where a pulsed electric current is used to join two faying surfaces, the above technology is assisted by plastic flow and solid state diffusion. The elemental distribution at the interface between the copper and the Ag-WC contact material is shown in Fig. 4. A clear diffusion layer (~40 μm) between the copper and the contact material can be observed, which was also retained after 50 switching operations.

3.3. SPS versus press-sinter-infiltrated Ag-WC-Ni composites

The microstructure of the three different Ag-WC-Ni (60-39.9-0.1 wt%) composites with varying WC particle sizes prepared by SPS (combined with powder treatment, Fig. 1(c) and Fig. 2(b)) and press-sinter-infiltration are shown in Fig. 5. The differences in homogeneity

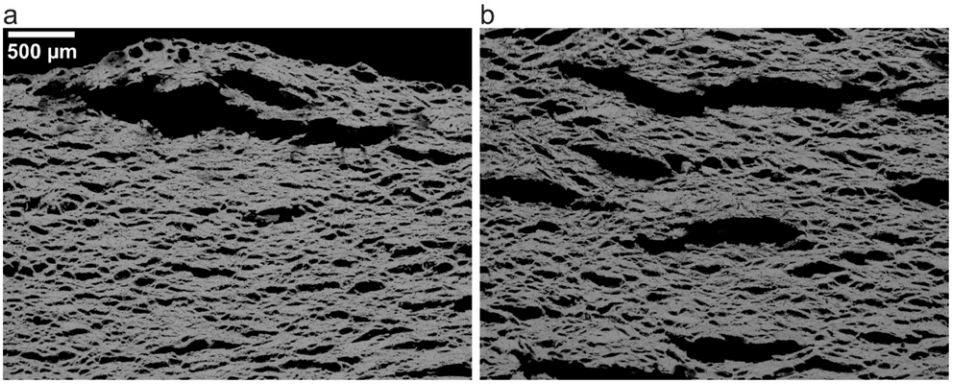

Fig. 3. Swelling of the as-milled solid state SPS composites after heat treatment for 1 h at (a) 990 °C and (b) 1070 °C in a H_2:N_2 (3:1) atmosphere.

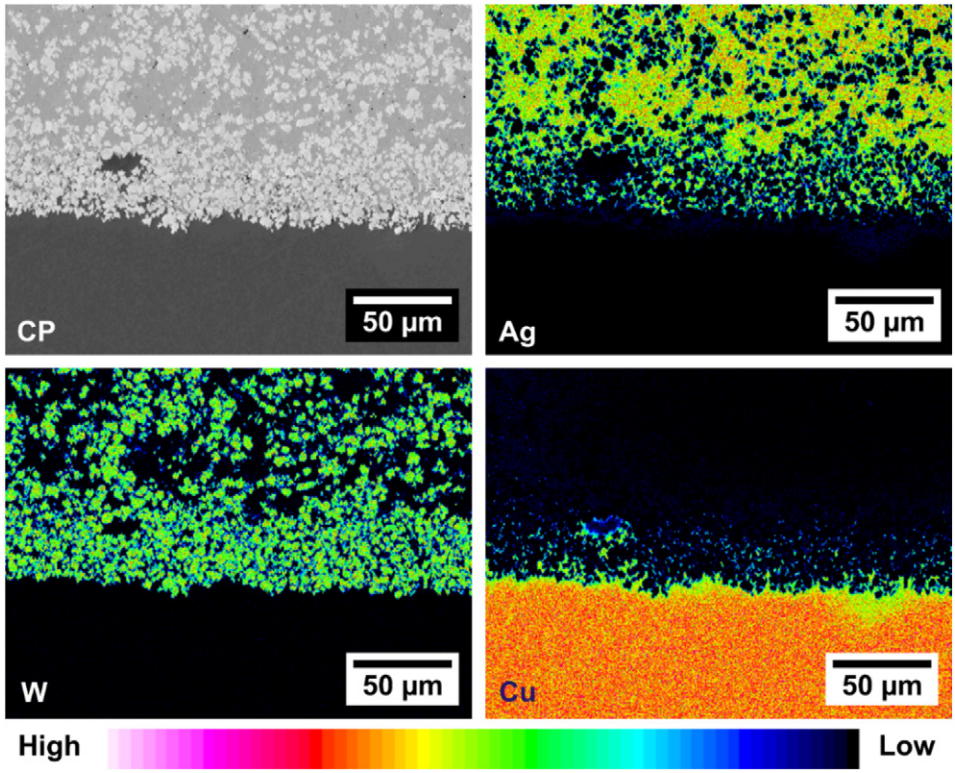

Fig. 4. Elemental mapping illustrating the in-situ formed interface between the copper plate and Ag-WC(4 μm)-Ni contact material during spark plasma sintering. CP or composition map shows the atomic number contrast of all the elements, similar to a backscattered electron image.

between SPS and infiltrated microstructures are clearer to distinguish in the material containing finer WC particles (Fig. 5(a)). The microstructure after SPS shows a more homogeneous phase distribution than after infiltration since the silver phase seems to have retained its original particle size of 5 μm with negligible agglomeration during sintering. However in the infiltrated material, the WC particles are more agglomerated compared to the SPS materials. During the sintering step, the silver present in the powder mixture binds together the WC particles and leaves behind large isolated pores which are later filled with silver during infiltration, leading to an inhomogeneous microstructure.

3.4. Mechanical properties

The flexural stress of the Ag-WC-Ni (60-39.9-0.1 wt%) SPS (Fig. 1(c) and Fig. 2(b)) and infiltrated Ag-WC composites as a function of flexural strain for the three different WC particle sizes are presented

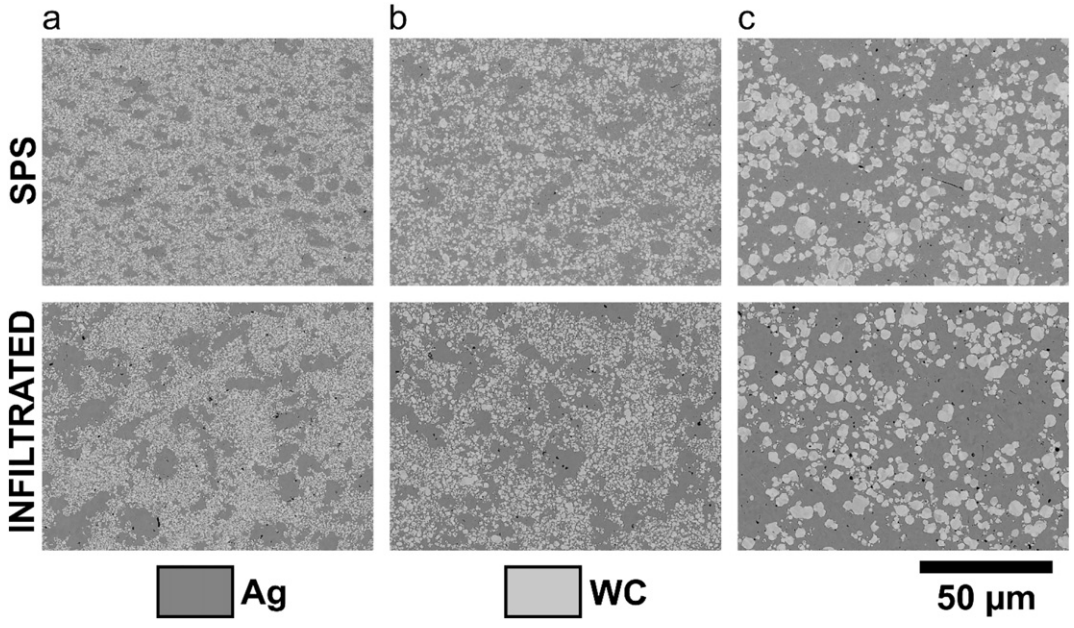

Fig. 5. Microstructure of Ag-WC-Ni (60-39.9-0.1 wt%) composites processed using spark plasma sintering and conventional press-sinter-infiltration for (a) 0.8 μm, (b) 1.5 μm and (c) 4 μm WC particle sizes (d_{50}).

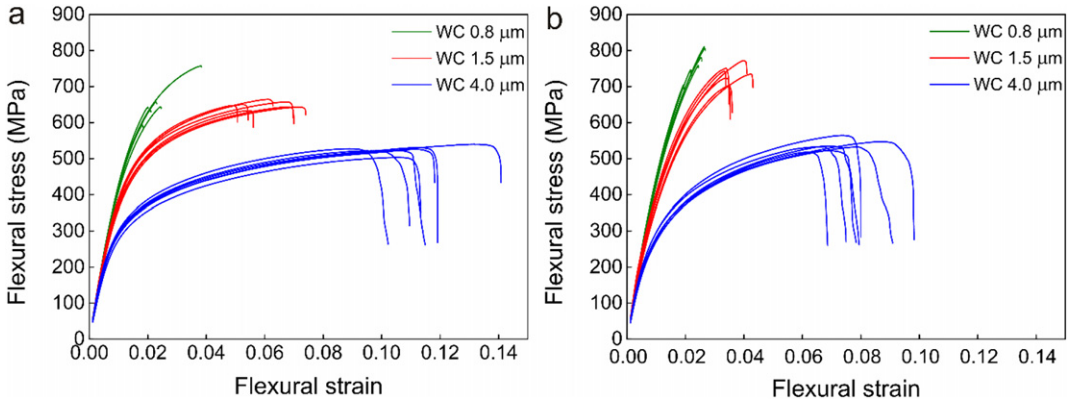

Fig. 6. Flexural stress-strain curves (3-point bending) of Ag-WC-Ni (60-39.9-0.1 Ni wt%) composites processed by (a) SPS and (b) conventional infiltration for different WC particle sizes (d_{50}).

in Fig. 6. The yield strength, failure strength, failure strain and toughness as determined from the curves are tabulated in Table 2. The Vickers hardness of the spark plasma sintered and press-sinter-infiltrated Ag-WC composites are also incorporated in Table 2. The toughness and failure strain of the Ag-WC composites increased with increasing WC particle size for both processing methods and the SPS materials were tougher and able to withstand higher strain until failure than their conventional infiltrated equivalents. Whereas, the failure strength and the hardness decreased with increasing WC particle size, the strength and hardness of the spark plasma sintered composites is consistently lower than for the infiltrated materials. Similarly, the yield offset point of the materials decreased with increasing WC particle size, and the SPS materials had a lower yield point with the exception of the WC 4 μm grade.

For a given processing method, the higher strength and hardness of the materials containing finer WC particles is due to grain boundary strengthening as demonstrated by the Hall-Petch relationship. However, in order to interpret the difference in hardness and strength of the SPS and infiltrated materials for a constant WC particle size, it is necessary to characterize the grain boundary type. Orientation imaging using electron backscattered diffraction (EBSD) was used since it is an appropriate tool to identify and classify grain boundaries. Fig. 7(a) and (b) show the inverse pole figure (IPF) maps showing the Ag and WC phases with grain boundaries having a misorientation ≥15°, thus defining a grain by high angle grain boundaries. Fig. 7(c) shows that the WC grain size for both SPS and infiltrated materials are similar but the Ag grain size in the SPS material is very small (~0.3 μm) compared to ~1 to 3 mm in the infiltrated materials (Fig. 7(c) (inset)). Although this should correspond to a higher hardness in the SPS materials as a consequence of grain boundary strengthening, the infiltrated materials have a higher hardness. This is because the infiltrated materials have a higher fraction of high angle (>15°) Ag/WC grain/phase boundaries compared to the SPS materials as shown in Fig. 7(d). This boils down to the fact that the dispersion strengthening of WC prevails the grain boundary strengthening of the Ag phase for a given WC particle size. The WC particles in the silver matrix act as incoherent dispersions and harden the parent matrix by Orowan looping [24], explaining the higher strength and hardness of the infiltrated material.

As shown in Fig. 5, the WC particles in the SPS materials are more homogeneously distributed in the Ag matrix than for the infiltrated materials. This leads to a larger inter-particle spacing between the dispersed WC particles in the SPS materials. Therefore, unlike in the infiltrated composites, the WC particles in the SPS composites do not sinter together (i.e. minimum particle-particle contact) leading to lower strength and hardness. Consequently, this high fraction of brittle WC-WC necks/boundaries (>15°, Fig. 7(d)) formed in the infiltrated materials leads to a lower toughness. Therefore, the most important result is that the difference between the strength or hardness of the SPS and infiltrated materials decreases with increasing WC particle size. This directly corresponds to the reduced neck formation between the WC particles with increasing particle size (Fig. 5) as a result of the lower driving force for sintering.

3.5. Arc-erosion and electrical contact resistance

The contact materials prepared by SPS made from a hydrogen treated powder (Fig. 1(c) and Fig. 2(b)), were tested in the break-only model switch and compared with the press-sinter-infiltrated contacts. Four identical Ag-WC composite discs were prepared for each pair of tests in which one disc was connected to the stationary electrode and the other to the movable electrode. Arc-erosion in the generic sense attributes to the 'material losses' after an arcing event. Usually, the material loss is due to boiling, liquid droplet expulsion and oxidation, yet in some cases brittle chunk expulsion can contribute to a major material loss [1,25]. However in DC applications, an important contributing factor is material transfer between the anode and the cathode [26–28]. Since arc-erosion is a complex phenomenon to monitor during each cycle, the weight loss of the contacts was measured after 50 switching cycles and divided by the total number of cycles. The arc-erosion measurement results are illustrated in Fig. 8, which compares the materials made by two processing routes for different WC particle sizes. The top half of the bar indicates the weight loss per cycle of the movable/upper contact whereas the bottom half of the bar expresses the weight loss of the stationary/lower contact. The arc-erosion resistance is best for the material containing the coarsest WC particles, which is due to the increase in ductility of the

Table 2
Mechanical properties of the Ag-WC-Ni (60-39.9-0.1 Ni wt%) composites with different WC starting powder size (d_{50}), processed by SPS and conventional infiltration.

Mechanical properties	SPS composites			Infiltrated composites		
	WC 0.8 μm	WC 1.5 μm	WC 4.0 μm	WC 0.8 μm	WC 1.5 μm	WC 4.0 μm
Yield strength (MPa)	452 ± 6	371 ± 5	259 ± 2	480 ± 8	376 ± 5	240 ± 5
Flexural failure strength (MPa)	655 ± 21	649 ± 4	524 ± 4	768 ± 15	738 ± 9	536 ± 6
Flexural failure strain (%)	2.4 ± 0.3	5.9 ± 0.3	10.7 ± 0.5	2.4 ± 0.1	3.6 ± 0.2	7.2 ± 0.3
Toughness in bending ($MJ \cdot m^{-3}$)	10.4 ± 1.9	31.0 ± 1.9	46.7 ± 2.6	11.1 ± 0.8	18.2 ± 0.9	30.2 ± 1.7
Hardness ($kg \cdot mm^{-2}$) ($HV_{0.3}$)	169 ± 2	140 ± 2	106 ± 2	212 ± 8	165 ± 5	116 ± 2

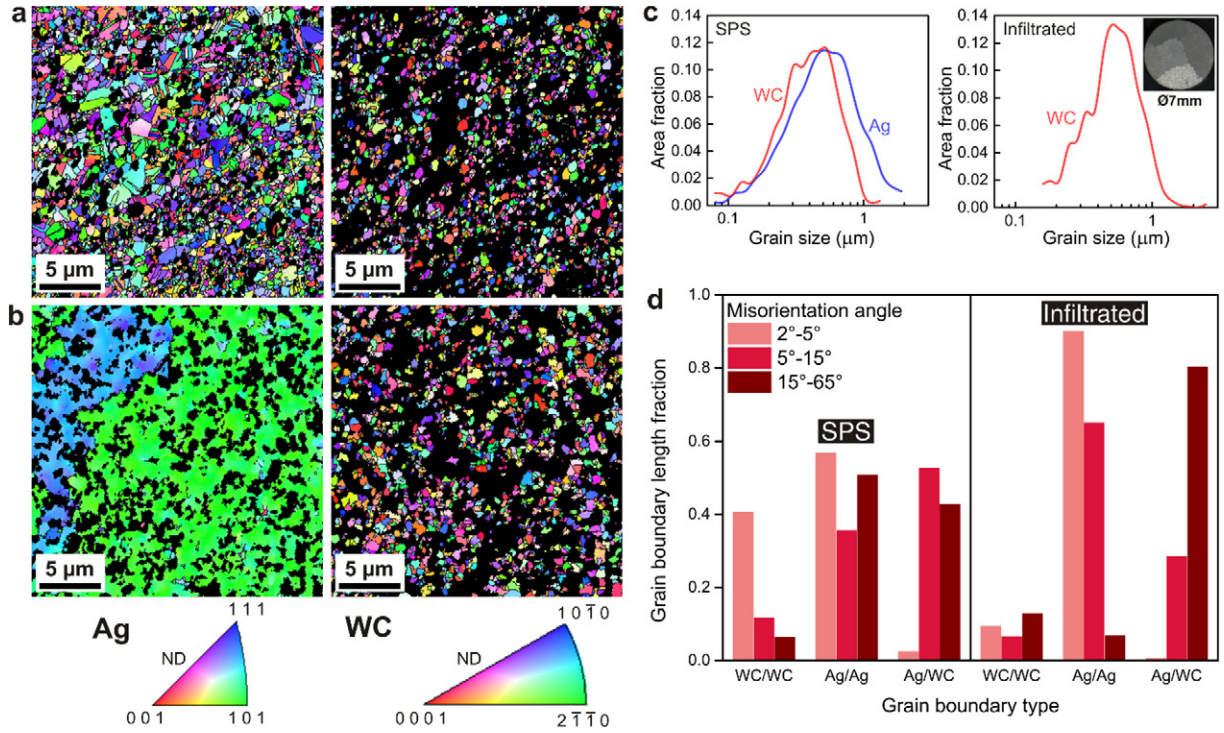

Fig. 7. Inverse pole figure maps showing the Ag and WC phases with grain boundaries having a misorientation ≥ 15° for the (a) SPS and (b) infiltrated Ag-WC(0.8 μm)-Ni contacts; (c) grain size distribution in the SPS and infiltrated materials, (inset) polarized light microstructure of top surface of a Ø 7 mm Ag-WC-Ni infiltrated disc showing the etched silver oligocrystals; (d) Grain boundary length fractions for SPS and infiltrated contact materials as a function of the misorientation angle.

contact material, independent of the material processing technology. The spark plasma sintered material however shows a lower arc erosion resistance than the infiltrated equivalent. This could be attributed to the preferential loss of silver by evaporation as discussed below, based on the microstructure after switching.

The electrical contact resistance (R_c) of the composites prepared by spark plasma sintering and infiltration follows a similar trend as compared in Fig. 9. The composites containing the coarsest WC (4 μm) phase have a significantly lower R_c in contrast to the materials with the finer WC (0.8 μm and 1.5 μm) particles. The large difference in contact resistance between the coarser WC (4 μm) and the finer WC (0.8 μm and 1.5 μm) can be explained from a combined effect of the percolating silver matrix and the flow stress of the surface layers formed during switching. As discussed earlier, the finer WC tends to agglomerate and limits the current carrying path through the WC phase. After a few cycles, the difference in contact resistance between the different WC particle sizes are clearer since a stable re-condensed surface layer is formed after each switching cycle. For the coarser WC containing materials, the surface layer is softer than for the finer WC, thus establishing a larger area of mechanical contact [1], leading to a lower contact resistance.

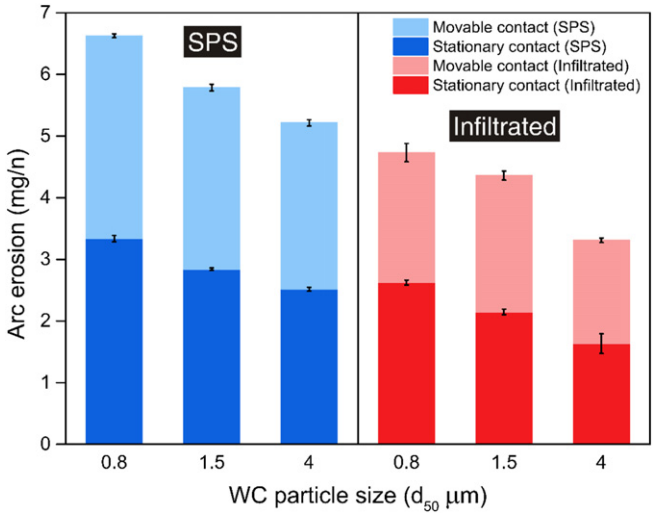

Fig. 8. Arc-erosion after 50 switching cycles attributed to the weight loss per switching cycle (n) of the upper/movable contact and lower/stationary contact for different WC particle sizes (d_{50}) processed using spark plasma sintering (blue) and conventional infiltration (red).

Fig. 10 shows the transverse section of the stationary contacts after 50 switching cycles. The infiltrated contacts were brazed on the copper rod whereas the SPS materials do not have a brazing layer in-between the contact and the copper. The interface between the contact material and the copper seems to sustain the arcing loads without any signs of major defects except for the material with WC 0.8 μm (Fig. 10(a)). The crack formation can be attributed to the lower thermal conductivity of the composite containing finer WC [15]. The * labelled micrographs are enlarged views of the top contact surface. The striking difference between the two processing routes is that the infiltrated material has major cracks in contrast to the SPS materials. The SPS grades however show a porous 'sponge' like contact surface in contrast to the infiltrated materials.

Cracks formed during electric arcing can be classified as vertical and horizontal cracks, based on their orientation to the surface of the contact [29]. The cracks are mainly attributed to thermal stresses related to the mismatch of thermal expansion coefficients between the constituent phases, thermal conductivity and the toughness of the composite. These cracks were only observed in the infiltrated materials, which are brittle and have the propensity to erode by *brittle chunk expulsion*. This directly correlates to the lower toughness (Table 2) of the infiltrated materials compared to the SPS materials. Although the cracks are absent in the materials prepared by SPS, they show porous structures on the contact surface in the form of sintered/re-condensed network of

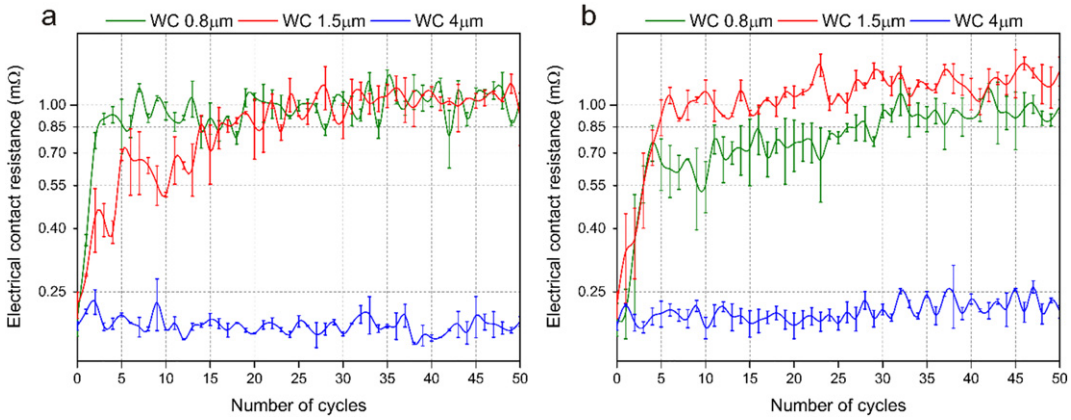

Fig. 9. Evolution of the electrical contact resistance (R_c) calculated from the voltage drop across the contacts over 50 switching cycles for different WC particle sizes (d_{50}) processed by SPS (a) and conventional infiltration (b).

Ag and WC (Fig. 11(a)). Despite the higher resistance to cracking and concomitant reduced loss of large parts of the SPS contacts, they show more material loss by the formation of a porous surface layer. The porous surface structure on the SPS materials is attributed to the preferential loss of silver by evaporation in comparison to the infiltrated materials. Fig. 11 shows a significant difference in microstructure between the arc-affected zone and the bulk of the SPS materials. In the heat affected region, the WC particles are more closely spaced compared to the bulk, consequently decreasing the thermal conductivity of the surface layer. This does not allow the heat on the surface to dissipate easily, leading to a preferential loss of silver at the contact surface.

4. Conclusions

Spark plasma sintering (SPS) was explored to densify Ag-WC-Ni (60-39.9-0.1 wt%) contact materials in comparison to the conventional press-sinter-infiltration process. SPS not only allowed to have a better control over the final silver content, but also minimized the number of processing steps compared to the conventional process. The Ag-WC-Ni composites were in-situ solid state welded to a copper substrate during SPS, eliminating an additional brazing step necessary in the conventional process. Based on the experimental results, the following conclusions can be drawn.

1. Ag-WC composites prepared by SPS from an as-mixed/milled powder mixture is fully dense. At temperatures above the melting point of silver (>962 °C) however, the dense body starts to swell and becomes porous (video in Supplementary material), rendering them unsuitable for arcing contact applications. This is due to the formation of water vapor and/or volatile oxides and oxyhydrates of tungsten at elevated temperatures (800–1200 °C) depending on the atmosphere during heat treatment.
2. In order to produce a stable Ag-WC electrical contact, a proper powder pretreatment, i.e. heat treatment at 945 °C for 8 h in the presence of hydrogen in order to reduce tungsten oxides, was necessary prior to SPS for 5 min at 750 °C and 80 MPa. The resultant composites had a density >99%, which was retained when heated above the melting point of silver.
3. The SPS composites had a more homogeneous microstructure but lower strength and hardness than their infiltrated counterparts, i.e. the 1.5 μm WC grade prepared by infiltration was 25 $HV_{0.3}$ harder than its SPS equivalent. The infiltrated materials had a larger fraction of high angle (>15°) Ag/WC phase/grain boundaries leading to dispersion strengthening. However, the SPS composites were tougher than their infiltrated equivalents, i.e. the 1.5 μm WC grade was 13 $MJ \cdot m^{-3}$ tougher than the material prepared by infiltration.

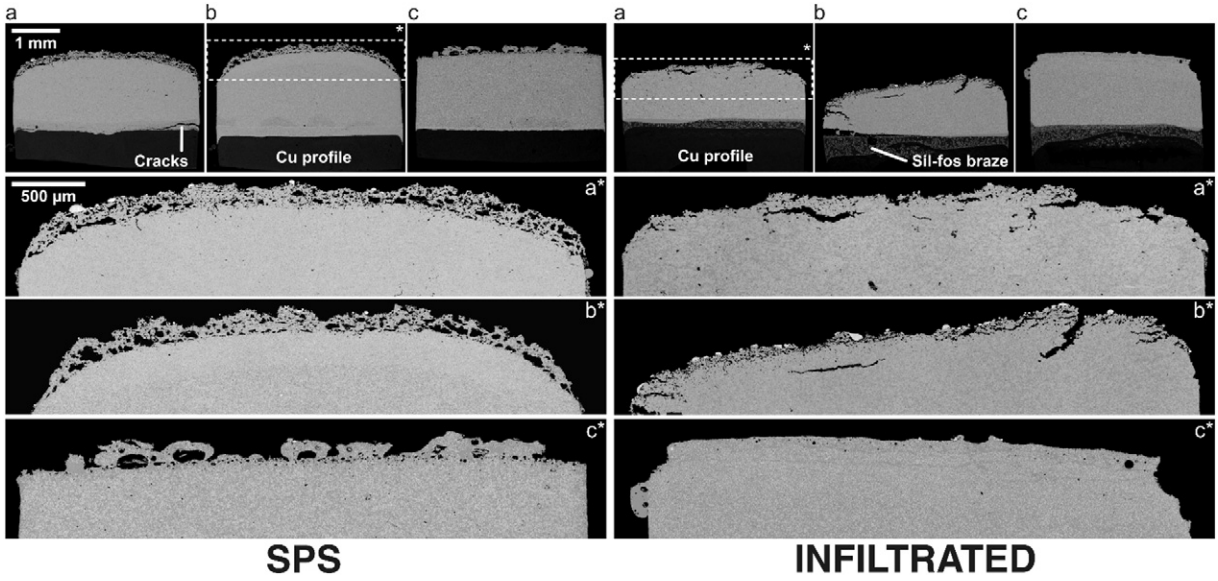

Fig. 10. Microstructure of the lower/stationary Ag-WC-Ni (60-39.9-0.1 wt%) contact after 50 switching cycles processed by spark plasma sintering and conventional infiltration for (a) 0.8 μm, (b) 1.5 μm and (c) 4 μm WC particle size (d_{50}).

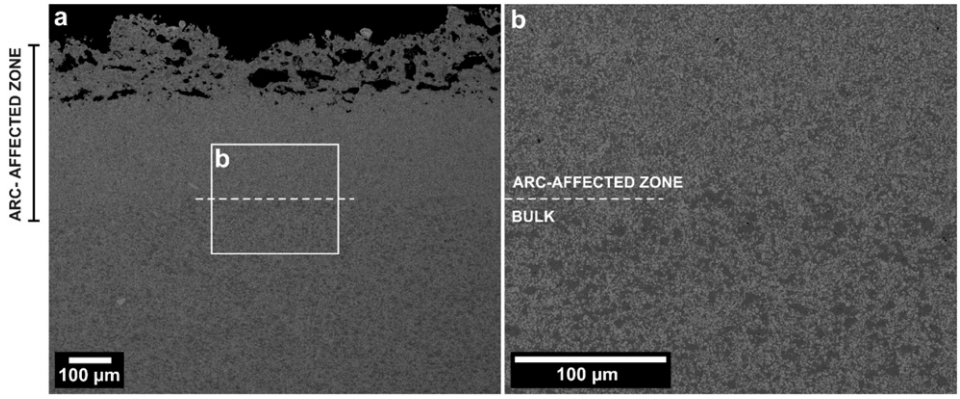

Fig. 11. Lower/stationary spark plasma sintered Ag-WC(1.5 μm)-Ni (60-39.9-0.1 wt%) contact material after 50 switching cycles, illustrating the difference in microstructure between the arc-affected zone and the bulk.

4. For a given processing method, the materials containing finer WC particles were stronger and harder, while being less tough, i.e. the SPSed 4 μm WC grade was 36 $MJ \cdot m^{-3}$ tougher than the 0.8 μm WC grade, but the hardness was 63 $HV_{0.3}$ lower. This was due to grain boundary strengthening of the composite containing finer WC particles as a result of the large fraction of WC grain boundaries.
5. The electrical contact resistance of both SPS and infiltrated materials was comparable, whereas the infiltrated materials showed a better arc-erosion resistance due to preferential evaporation of silver from the contact surface of the SPS materials.
6. Both the electrical contact resistance and arc-erosion decreased with increasing WC particle size for a given processing method. Contact resistance decreases due to increased ductility whereas arc-erosion decreases due to increased thermal conductivity.
7. The microstructure of the switched contacts also divulged that the SPS materials were free of cracks in contrast to their infiltrated counterparts. The surface of the SPS materials displayed a porous 'sponge' like microstructure which was attributed to the preferential evaporation of silver. This was due to the difference in thermal conductivity between the arc-affected zone and the bulk, which constrained the heat dissipation away from the contact surface.

Supplementary data to this article can be found online at http://dx.doi.org/10.1016/j.matdes.2017.02.070.

Acknowledgements

The authors gratefully acknowledge support from the Flemish government via the Hercules Foundation (project ZW09-09) for the electron probe micro-analyzer and the NanoSEM. The authors greatly appreciate the help from Christian Hubrich from Technical Materials, Umicore, Germany for his assistance with the break-only model switching device and Dr. Jan De Munck from the Department of Oral Health Sciences, KU Leuven, Belgium for his assistance with the bending tests.

References

[1] P.G. Slade, Electrical Contacts: Principles and Applications, CRC Press, 1999.
[2] C.-H. Leung, Arcing contact materials, silver refractory metals, in: Q.J. Wang, Y.-W. Chung (Eds.), Encyclopedia of Tribology, Springer US 2013, pp. 104–107, http://dx.doi.org/10.1007/978-0-387-92897-5_404.
[3] P.G. Slade, The switching performance of refractory carbide-silver contacts, IEEE Transactions on Components, Hybrids, and Manufacturing Technology, 2, 1979, pp. 127–133, http://dx.doi.org/10.1109/TCHMT.1979.1135409.
[4] M. Madej, Silver – based infiltrated composites, Arch. Metall. Mater. 57 (2012) 605–612, http://dx.doi.org/10.2478/v10172-012-0064-x.
[5] M. Osadnik, M. Czepelak, M. Kamińska, Production and Properties of AgW50 Composites Designated for Electric Contacts, 2014.
[6] M. Vijayakumar, A.M. Sriramamurthy, S.V. Nagender Naidu, Calculated phase diagrams of Cu-W, Ag-W and Au-W binary systems, Calphad 12 (1988) 177–184, http://dx.doi.org/10.1016/0364-5916(88)90019-3.
[7] Q. Xiong, S. Wang, M. Xie, Y. Chen, J. Zhang, S. Wang, AgSnO2 Electrical Contact Material Prepared by Spark Plasma Sintering, Precious Metals, 34, 2013http://dx.doi.org/10.3969/j.issn.1004-0676.2013.04.003.
[8] N. Amandine, K. Ayala, A. Ludovic, F. Gilbert, B. Guillaume, Sinterability of Low Voltage Contact Materials, in: Lausanne, Switzerland, 2008 177.
[9] M. Lungu, V. Tsakiris, E. Enescu, D. Pătroi, V. Marinescu, D. Tălpeanu, D. Pavelescu, G. Dumitrescu, A. Radulian, Development of W-Cu-Ni electrical contact materials with enhanced mechanical properties by spark plasma sintering process, Acta Phys. Pol. A 125 (2014) 327–330, http://dx.doi.org/10.12693/APhysPolA.125.327.
[10] V. Tsakiris, E. Enescu, M. Lungu, M. Lucaci, A. Radulian, D. Talpeanu, G. Sbarcea, A. Caramitu, V. Marinescu, I. Ioana, Electrical Contact Materials Obtained by Spark Plasma Sintering Technology for Vacuum Contactors, 2015 490–495, http://dx.doi.org/10.1109/ATEE.2015.7133851.
[11] M. Alvarez, J.M. Sánchez, Spark plasma sintering of Ti(C, N) cermets with intermetallic binder phases, Int. J. Refract. Met. Hard Mater. 25 (2007) 107–118, http://dx.doi.org/10.1016/j.ijrmhm.2006.03.004.
[12] W.T. Allen, Electrical Contact, US2298999 (A), http://worldwide.espacenet.com/publicationDetails/biblio?FT=D&date=19421013&DB=EPODOC&locale=en_EP&CC=US&NR=2298999A&KC=A&ND=4 1942 (accessed April 8, 2016).
[13] W.T. Allen, Electrical Contact, US2299000 (A), http://worldwide.espacenet.com/publicationDetails/biblio?FT=D&date=19421013&DB=&locale=&CC=US&NR=2299000A&KC=A&ND=1 1942 (accessed April 11, 2016).
[14] C. Jiang, H. Chen, Q. Wang, Y. Li, Effect of brazing temperature and holding time on joint properties of induction brazed WC-Co/carbon steel using Ag-based alloy, J. Mater. Process. Technol. 229 (2016) 562–569, http://dx.doi.org/10.1016/j.jmatprotec.2015.09.044.
[15] N. Ray, B. Kempf, T. Mützel, L. Froyen, K. Vanmeensel, J. Vleugels, Effect of WC particle size and Ag volume fraction on electrical contact resistance and thermal conductivity of Ag–WC contact materials, Mater. Des. 85 (2015) 412–422, http://dx.doi.org/10.1016/j.matdes.2015.07.006.
[16] K. Vanmeensel, A. Laptev, J. Hennicke, J. Vleugels, O. Van der Biest, Modelling of the temperature distribution during field assisted sintering, Acta Mater. 53 (2005) 4379–4388, http://dx.doi.org/10.1016/j.actamat.2005.05.042.
[17] ASTM C20-00(2015), Standard Test Methods for Apparent Porosity, Water Absorption, Apparent Specific Gravity, and Bulk Density of Burned Refractory Brick and Shapes by Boiling Water, ASTM International, West Conshohocken, PA, 2015www.astm.org10.1520/C0020-00R15.
[18] P. Pongprueksa, J.D. Munck, K. Karunratanakul, B.C. Barreto, A.V. Ende, P. Senawongse, B.V. Meerbeek, Dentin bonding testing using a mini-interfacial fracture toughness approach, J. Dent. Res. 95 (2016) 327–333, http://dx.doi.org/10.1177/0022034515618960.
[19] N. Ray, B. Kempf, T. Mützel, F. Heringhaus, L. Froyen, K. Vanmeensel, J. Vleugels, Effect of Ni addition on the contact resistance of Ag-WC electrical contacts, J. Alloys Compd. 670 (2016) 188–197, http://dx.doi.org/10.1016/j.jallcom.2016.02.037.
[20] C. Wilson, G. McIntosh, R.S. Timsit, Contact spot temperature and the temperature of external surfaces in an electrical connection, 26th International Conference on Electrical Contacts (ICEC 2012) 2012, pp. 12–17, http://dx.doi.org/10.1049/cp.2012.0614.
[21] G. Meyer, J.F. Oosterom, W.J. van Oeveren, The vapour pressure of tungsten trioxide in gas mixtures containing water vapour, Recl. Trav. Chim. Pays-Bas. 78 (1959) 417–423, http://dx.doi.org/10.1002/recl.19590780606.
[22] E. Lassner, W.-D. Schubert, Tungsten: Properties, Chemistry, Technology of the Elements, Alloys, and Chemical Compounds, Springer Science & Business Media, 1999.
[23] C. Fu, J. Hou, J. Wang, M. Yang, X. He, X. Su, S. Liu, X. Hu, Preparation Method of Silver Tungsten Carbide Contact Alloy, CN103290359 (A), https://worldwide.espacenet.com/publicationDetails/biblio?FT=D&date=20150708&DB=

&locale=&CC=CN&NR=103290359B&KC=B&ND=1 2015 (accessed July 18, 2016).
[24] D. Hull, D.J. Bacon, Introduction to Dislocations, Butterworth-Heinemann, 2001.
[25] C. Wu, D. Yi, W. Weng, S. Li, J. Zhou, Influence of alloy components on arc erosion morphology of Ag/MeO electrical contact materials, Trans. Nonferrous Metals Soc. China 26 (2016) 185–195, http://dx.doi.org/10.1016/S1003-6326(16)64105-5.
[26] C. Wu, D. Yi, W. Weng, S. Li, J. Zhou, F. Zheng, Arc erosion behavior of Ag/Ni electrical contact materials, Mater. Des. 85 (2015) 511–519, http://dx.doi.org/10.1016/j.matdes.2015.06.142.
[27] H. Li, X. Wang, X. Guo, X. Yang, S. Liang, Material transfer behavior of AgTiB2 and AgSnO2 electrical contact materials under different currents, Mater. Des. 114 (2017) 139–148, http://dx.doi.org/10.1016/j.matdes.2016.10.056.
[28] H. Li, X. Wang, Y. Liu, X. Guo, Effect of strengthening phase on material transfer behavior of Ag-based contact materials under different voltages, Vacuum 135 (2017) 55–65, http://dx.doi.org/10.1016/j.vacuum.2016.10.031.
[29] P.C. Wingert, Testing of the thermal-stress-cracking characteristics of silver-refractory contacts, Proceedings of the Forty-first IEEE Holm Conference on Electrical Contacts, 1995 1995, pp. 338–345, http://dx.doi.org/10.1109/HOLM.1995.482889.